Supplementary Information

Conserved catalytic motifs encode enzyme-like supramolecular peptide assemblies

Table S1 | Summary of protein sequences used for evolutionary conservation analysis. Homologous sequences were identified using the NIH BLAST server and grouped by enzyme class and taxonomic kingdom prior to multiple sequence alignment.

Enzyme class	Kingdom	Homologous sequences
Carbonic anhydrase	Animals	1,648
Carbonic anhydrase	Archaea	31
Carbonic anhydrase	Bacteria	1,051
Carbonic anhydrase	Fungi	251
Carbonic anhydrase	Plants	251
Carbonic anhydrase	Protists	66
Cu-containing superoxide dismutase (CuSOD)	Animals	4,183
Cu-containing superoxide dismutase (CuSOD)	Archaea	61
Cu-containing superoxide dismutase (CuSOD)	Bacteria	5,004
Cu-containing superoxide dismutase (CuSOD)	Protists	2,927
Cu-containing superoxide dismutase (CuSOD)	Fungi	1,594
Cu-containing superoxide dismutase (CuSOD)	Plants	1,826
Cu/Zn superoxide dismutase (Cu/ZnSOD)	Animals	4,999
Cu/Zn superoxide dismutase (Cu/ZnSOD)	Archaea	65
Cu/Zn superoxide dismutase (Cu/ZnSOD)	Bacteria	5,000
Cu/Zn superoxide dismutase (Cu/ZnSOD)	Protists	3,733
Cu/Zn superoxide dismutase (Cu/ZnSOD)	Fungi	1,833
Cu/Zn superoxide dismutase (Cu/ZnSOD)	Plants	2,202

Fig. S1 | Multiple sequence alignments of the XHXHX zinc binding site of carbonic anhydrase. Sequences from a) Archaea b) Bacteria c) Protista d) Fungi e) Plants f) Animals

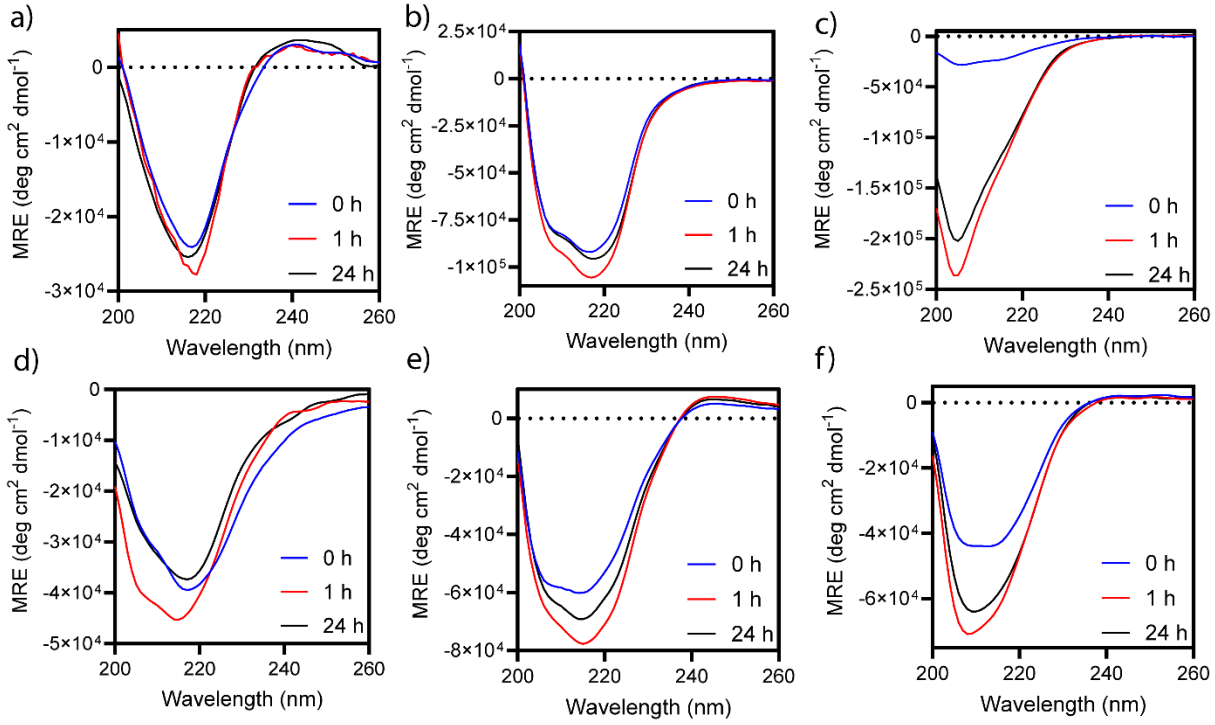

Fig. S2 | Circular dichroism spectra of the studied peptides collected at various time points upon self-assembly. a) Ac-QFHFHWG-NH_2 b) Ac-FHFHFQF-NH_2 c) Ac-FQFHFHF-NH_2 d) Ac-FHFHFYF-NH_2 e) Ac-FYFHFHF-NH_2 f) Ac-FYFHFHFQF-NH_2. All measurements were done in 5 mM HEPES, pH 8, with 100 µM peptide, 100 µM Zn^{2+}.

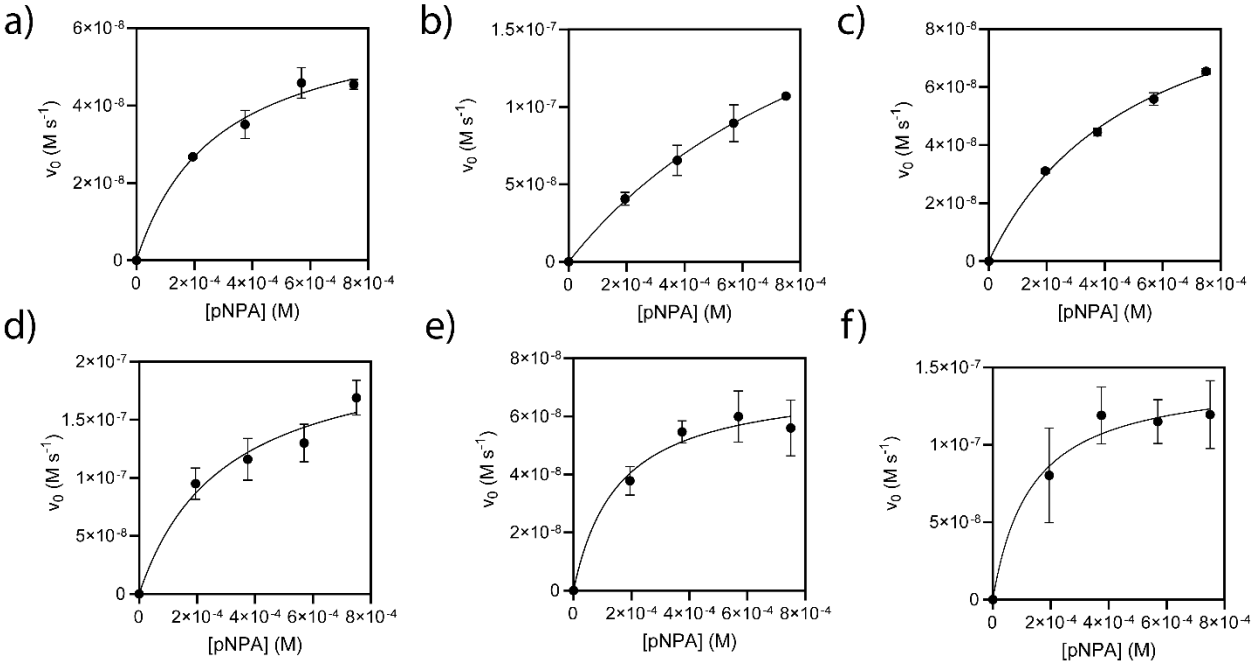

Fig. S3 | Dependence of the initial rate of hydrolysis on the concentration of paranitrophenyl acetate, with the results fit to the Michaelis-Menten equation. a) Ac-QFHFHWG-NH_2 b) Ac-FHFHFQF-NH_2 c) Ac-FQFHFHF-NH_2 d) Ac-FHFHFYF-NH_2 e) Ac-FYFHFHF-NH_2 f) Ac-FYFHFHFQF-NH_2. 25 µM peptide, 25 µM Zn, 25 mM Tris, pH 8.

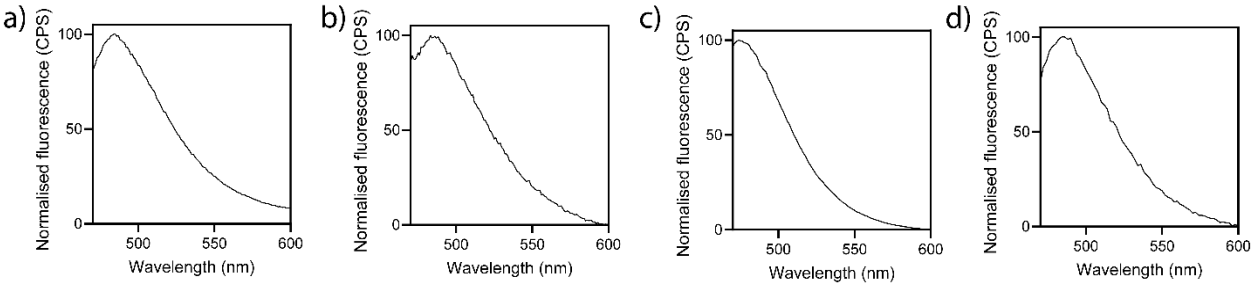

Fig. S4 | Fluorescence assays showing the increase in fluorescence of thioflavin T in the presence of peptide samples (baseline subtracted). 100 µM peptide, 25 µM ThT, 25 mM Tris, pH 8. a) Ac-FHFHFQF-NH_2 b) Ac-FQFHFHF-NH_2 c) Ac-FHFHFYF-NH_2 d) Ac-FYFHFHF-NH_2

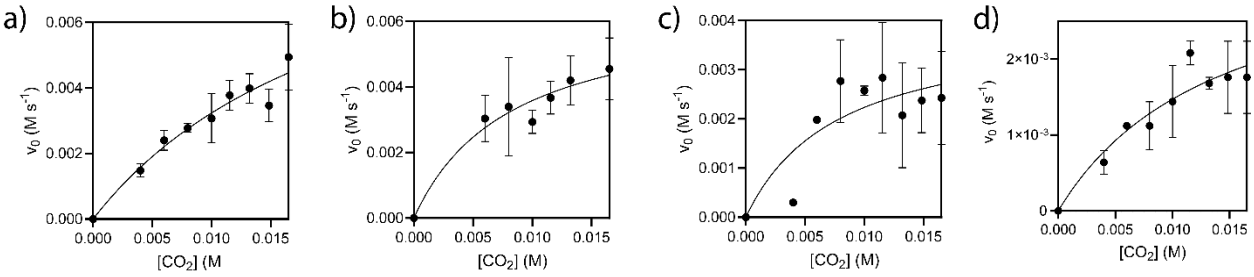

Fig. S5 | Dependence of the rate of carbon dioxide hydration on substrate concentration, with the results fit to the Michaelis-Menten equation. a) Ac-FHFHFQF-NH_2 b) Ac-FQFHFHF-NH_2 c) Ac-FHFHFYF-NH_2 d) Ac-FYFHFHF-NH_2. 2.5 µM peptide, 2.5 µM Zn, 50 mM CHES, pH 9.5, 25 µM thymol blue.

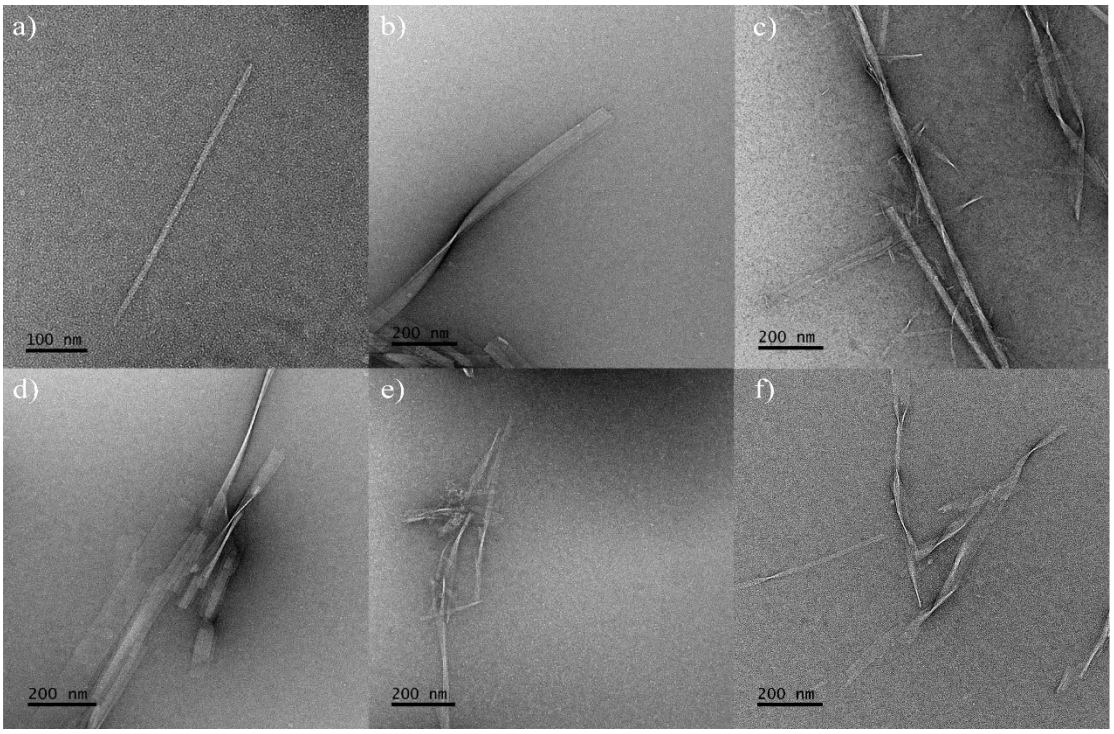

Fig. S6 | Transmission electron micrographs of a) Ac-QFHFHWG-NH_2 b) Ac-FQFHFHF-NH_2 c) Ac-FHFHFQF-NH_2 d) Ac-FYFHFHF-NH_2 e) Ac-FHFHFYF-NH_2 f) Ac-FYFHFHFQF-NH. 25 mM Tris, pH 8, 100 µM peptide, 100 µM Zn.

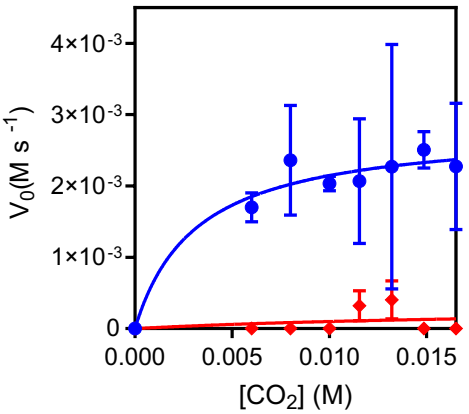

Fig. S7 | CO_2 hydration catalytic activity before (blue) and after (red) amyloid fibrils were subjected to ultracentrifugation. 2.5 uM Ac-QFHFHWG-NH_2, 2.5 uM Zn, 50 mM CHES pH 9.5

Table S2| CryoEM data collection and processing statistics

Data collection and processing	
Microscope	Titan Krios
Acceleration Voltage (kV)	300
Camera	K3
Nominal magnification	105,000x
Dose rate (e^- /pixel/s)	18
Total electron dose ($e^-/Å^2$)	50
Defocus range (μm)	-0.8 to -2.2
Pixel size (Å)	0.827
Symmetry imposed	C2
Particles after 2D (no.)	990,463
Final particles (no.)	37,444
Map resolution, 0.143 FSC criterion (Å)	2.3
Helical twist (°)	-2.97
Helical rise (Å)	4.76
Refinement	
Initial model used	*De Novo*
Model composition	
Non-H atoms	2063
Protein residues	112
Ligand	ACE:16, NH2:16
R.m.s. deviations	
Bond lengths (Å)	0.007

Bond angles (°)	0.933
CC (volume/mask)	0.78/0.78
CC for ligands	0.74
Validation	
MolProbity score	1.28
Clashscore	3.88
Poor rotamers (%)	0.00
Ramachandran plot	
Favored (%)	97.50
Allowed (%)	2.50
Disallowed (%)	0.00
PDB/EMDB code	

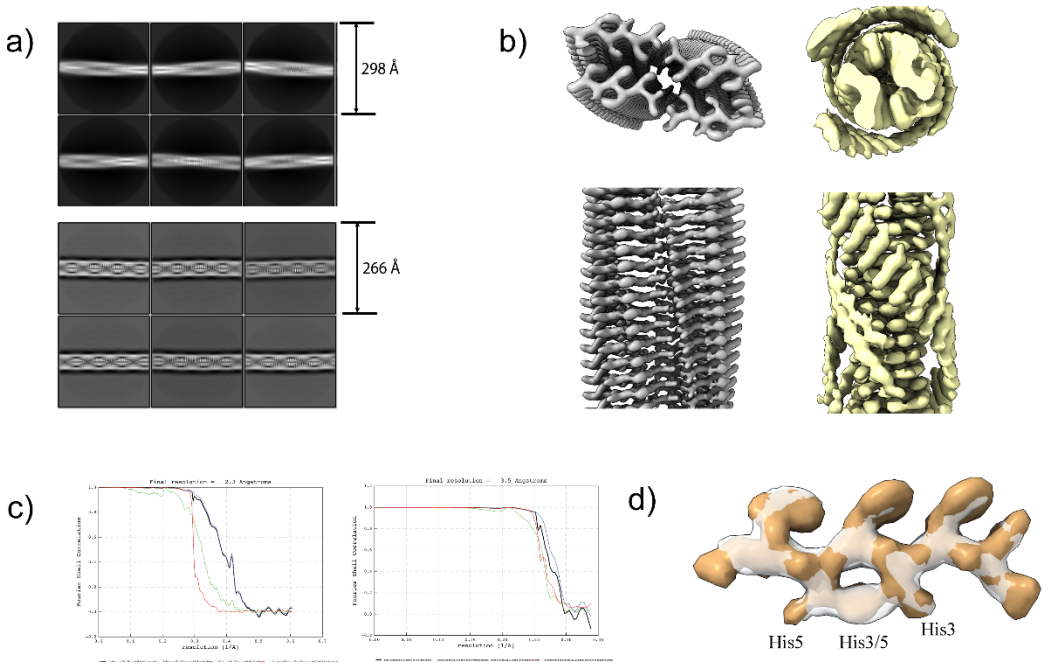

Fig. S8 | CryoEM analysis of 1-Zn^{2+} compared to previously published apo 1 map.(*82*) a) Cryo-EM 2D class averages showing distinct morphologies of Zn-bound (top) and apo (bottom) Ac-QFHFHWG-NH_2 fibrils. b) Top and side views of the cryo-EM density maps of Zn-bound and apo fibrils, highlighting the substantial conformational differences. c) Fourier shell correlation (FSC) curves for the Zn-bound (left) and apo (right) structures, as calculated by Relion Post-processing. d) Overlay of

the experimental cryo-EM density map (silver) with an averaged map generated from the two models taking on alternative conformations at Histidine 3 and Histidine 5, as shown in Fig. 2A, filtered to 2.3 Å resolution (orange). The shape of the cryo-EM density map can be well-accounted for by an average of the two conformations.

Table S3 | ^{111m}Cd PAC parameters for Cd(II) bound to QFHFHWG peptide amyloids. 100 mM Hepes, pH 7.7, 2 mM QFHFHWG, 0.1 mM $CdCl_2$, 20 °C.

ω_0 **rad/ns**	η	δ **×100**	λ **μs^{-1}**	A **×100**
0.069(1)	0.30(2)	3(2)	6(1)	8.1(3)

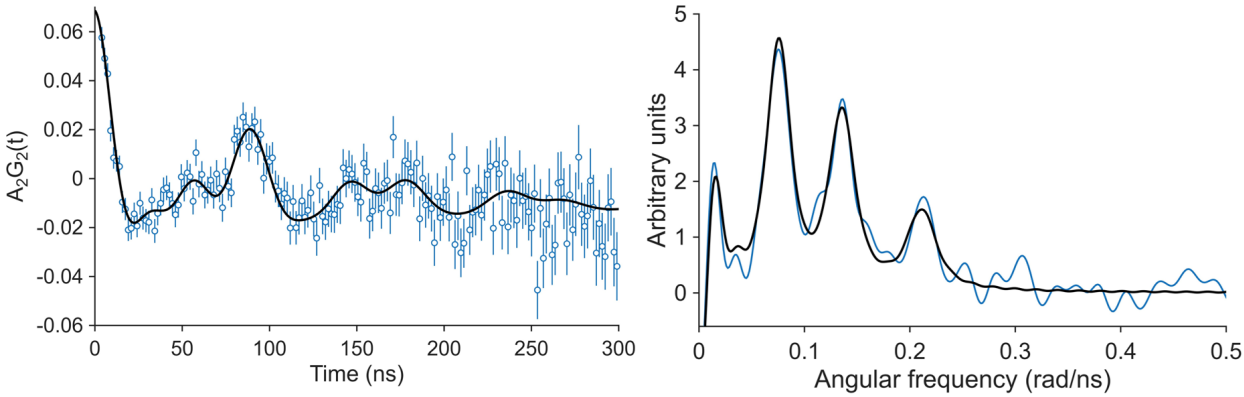

Fig. S9 | ^{111m}Cd PAC data for Cd(II) bound to QFHFHWG peptide amyloids. Left panel: Fitted perturbation function (full line), and data with error bars, plotted as a three-point average to facilitate visual inspection. Right panel: Fourier transformed fit (black line) and data (blue line). Sample conditions: 100 mM HEPES, pH 7.7, 2 mM Ac-QFHFHWG-NH_2, 0.1 mM $CdCl_2$, 20 °C. One well defined NQI adequately describes the data under these conditions with sub-equimolar amounts (0.05 eq.) of Cd(II) with respect to the peptides. See Table S3 for the fitted PAC parameters.

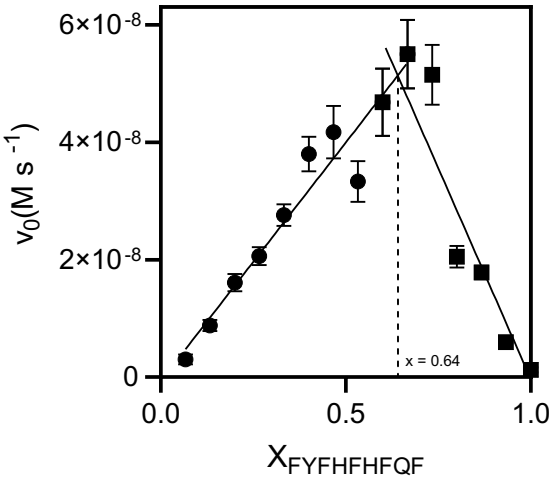

Fig. S10 | pNPA hydrolysis to determine metal-amyloid stoichiometry, using the method of continuous variation (Job's plot). The total concentration of Ac-FYFHFHFQF-NH_2 and Zn^{2+} was kept at 25 μM, 375 μM pNPA, 25 mM Tris, pH 8.

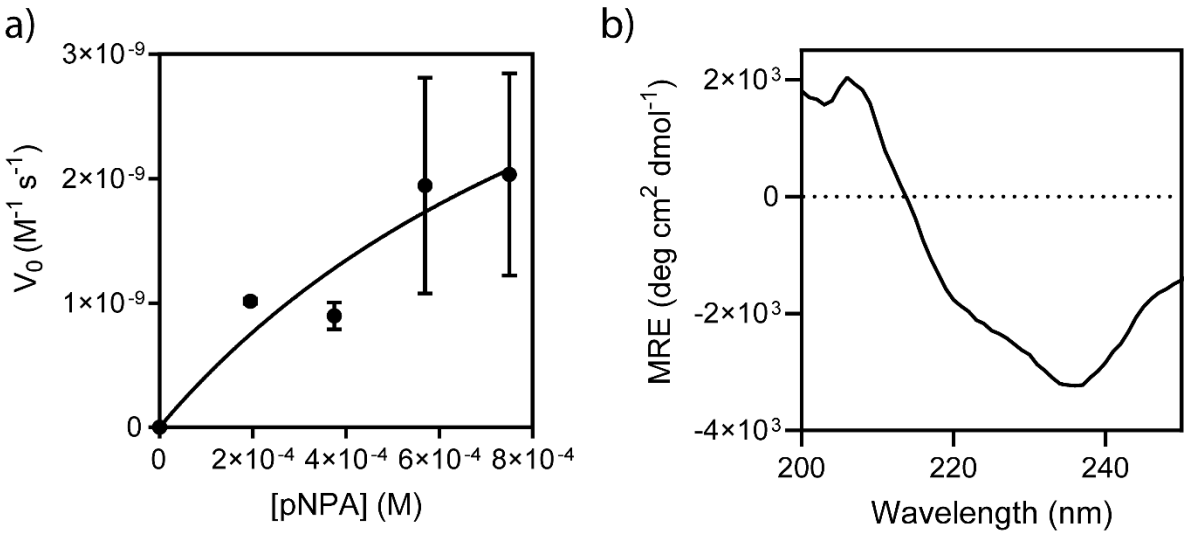

Fig. S11 | Characterization of Ac-FYF$_{NMe}$HF$_{NMe}$HFQF-NH$_2$. a) Michaelis-Menten plot for pNPA hydrolysis. 25 µM peptide, 25 µM Zn^{2+}, 25 mM Tris pH 8. B) Circular dichroism spectra 100 µM peptide, 100 µM Zn^{2+}, 5 mM HEPES pH 8

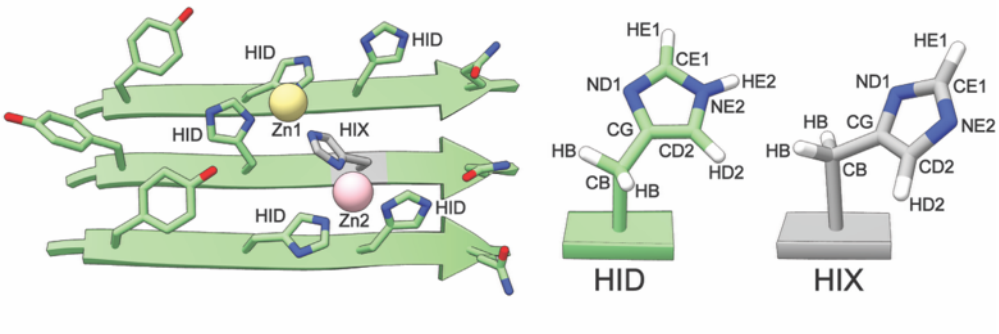

Fig. S12 | Models of Zn^{2+}-HIS_3 core and neutral (HID) and charged (HIX) forms of HIS.

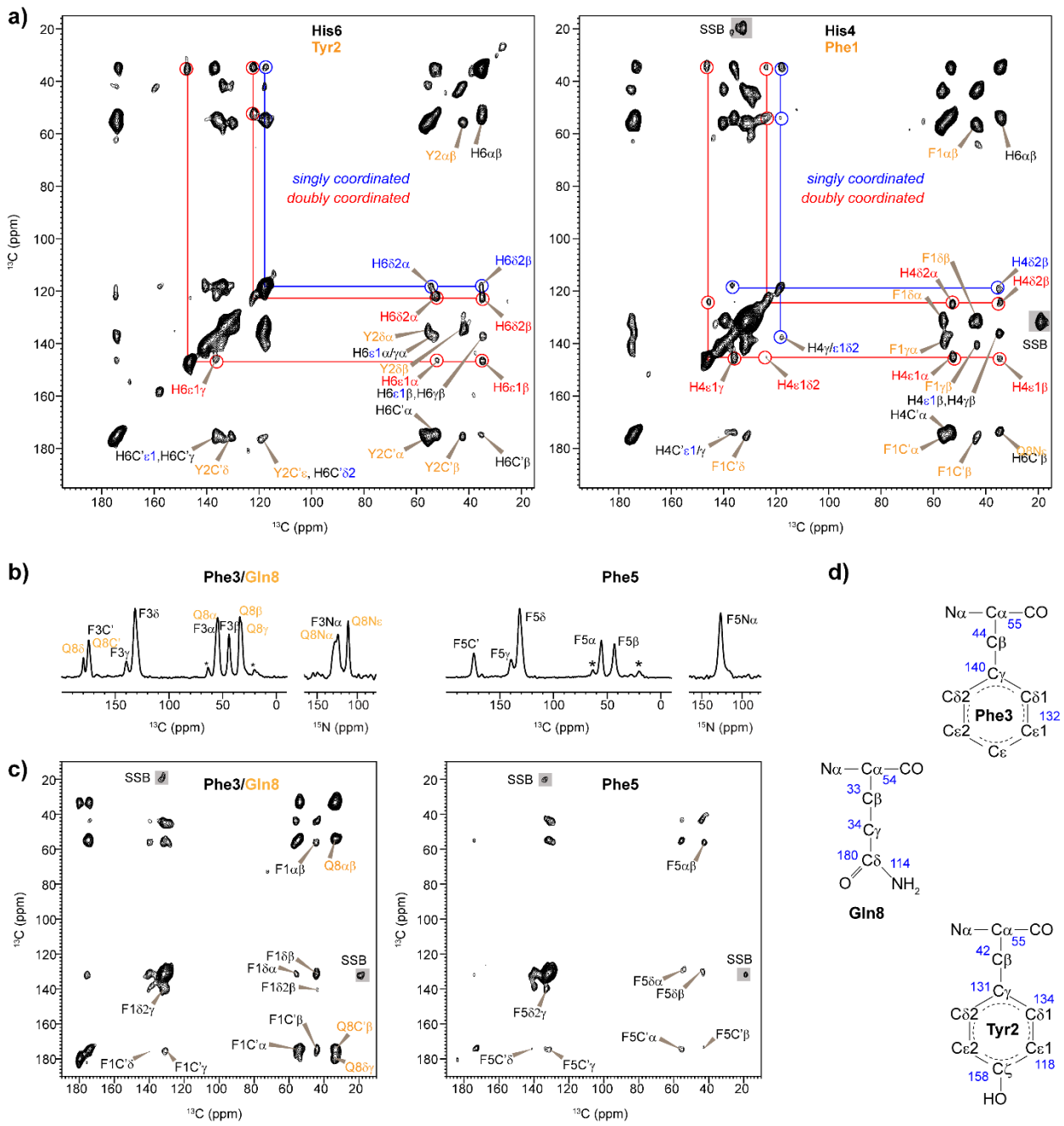

Fig. S13 | Resonance assignment from 1D ^{13}C, ^{15}N spectra and 2D ^{13}C-^{13}C correlation spectra. a) 2D ^{13}C-^{13}C correlation spectra measured on Y2H4 (left) and F1H4 (right) fibrils for identifying the singly (blue) and doubly (red) coordinated His residues. SSB: spinning sidebands. b) 1D ^{13}C and spectra of F3Q8 fibril (right) and F5 fibril (right) showing the resonance assignments for Phe3, Gln8, and Phe5. c) 2D ^{13}C-^{13}C correlation spectra of F3Q8 fibril (right) and F5 fibril (right). d) Summary of chemical shifts of Phe3, Tyr2, and Gln8.

Fig. S14 | Multiple sequence alignments of the copper binding site of Cu-superoxide dismutase. Sequences from a) Archaea b) Bacteria c) Protista d) Fungi e) Plants f) Animals

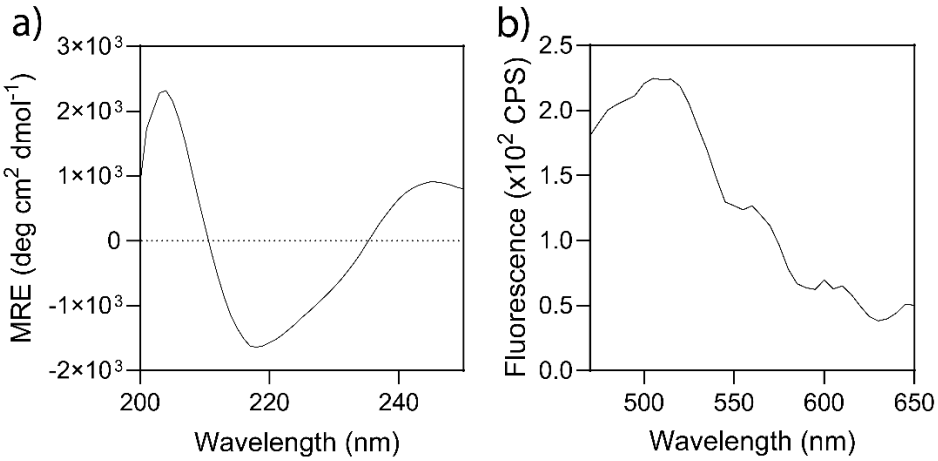

Fig. S15 | a) Circular dichroism spectrum of Ac-HGIHIH-NH_2 in the presence of copper. 100 µM Ac-HGIHIH-NH_2, 100 µM Cu^{2+}, 5 mM HEPES pH 7.8 b) Fluorescence assay showing the increase in fluorescence of thioflavin T in the presence of peptide Ac-HGIHIH-NH_2 (baseline subtracted). 100 µM peptide, 100 µM Cu^{2+}, 25 µM ThT, 5 mM HEPES, pH 7.8

Table S4 | Superoxide dismutase activity of previously reported peptide models

	Metal	IC_{50} (nM)	k_{McF} x10^9 (M^{-1} s^{-1})	Method	pH	Ref
SOD	Cu/Zn	4.5	1.2	Pulse Radiolysis	7.0	[1]
SOD	Fe	n.r.	3.25	KO_2 or XO	7.8	[2]
SOD	Mn	n.r.	3.78	KO_2 or XO	7.8	[2]
SOD	Ni	n.r.	1.3	KO_2	7.0	[3]
SOD	Cu	n.r.	1.1-1.8	Pulse Radiolysis	6.0	[1]
Ac-PDHKHHKH-NH_2	Cu	124	0.024	XO/XTT	7.5	[4]
Cyclic(HKHGPG)$_2$	Cu/Zn	360	n.r.	XO/NBT	7.4	[5]
Ac-HAAHVH-NH_2	Cu	77	n.r.	XO/NBT	7.4	[6]
Ac-HAAHGH-NH_2	Cu	480	n.r.	XO/NBT	7.4	[6]
Ac-HGGH-NH_2	Cu	380	n.r.	XO/NBT	7.4	[6]

Ac-HGGGHGH-NH_2	Cu	82	n.r.	XO/NBT	7.4	[6]
Ac-HVVH-NH_2	Cu	630	n.r.	XO/NBT	7.4	[6]
Ac-HHGH-NH2	Cu	170	n.r.	XO/NBT	7.4	[6]
Ac-HAHPH-NH_2	Cu	120	n.r.	XO/NBT	7.4	[6]
Ac-HGGGHGH-NH_2	Cu	71	n.r.	XO/NBT	7.4	[6]
Ac-HHGH-NH_2	Cu	130	n.r.	XO/NBT	7.4	[6]
Ac-HKHKH-NH_2	Cu	650	n.r.	XO/NBT	7.8	[7]
Ac-HHKHKH-NH_2	Cu	500	n.r.	XO/NBT	7.2	[7]
HADHDHKK-NH_2	Cu	110	n.r.	XO/NBT	7.0	[7]
Ac-RHQAGPPHSHR-NH_2	Cu	100	n.r.	XO/NBT	7.4	[7]
HHDLPCGVY-NH_2	Ni	37,000	7.2×10^{-5}	XO/NBT	7.8	[8]
HCDLPHGVY-NH_2	Ni	341,000	7.9×10^{-6}	XO/NBT	7.8	[8]
H-HADHDHKK-NH_2	Cu	n.r.	2.7×10^{-3}	XO/NBT	7.8	[9]
GRα_3D H_3	Cu	2900	3×10^{-3}	XO/XTT	7.5	[10]
GRα_3D H_4	Cu	8000	1.1×10^{-3}	XO/XTT	7.5	[10]
GRα_3D H_2DH	Cu	3500	2.6×10^{-3}	XO/XTT	7.5	[10]
GRα_3D H_3D	Cu	3300	2.6×10^{-3}	XO/XTT	7.5	[10]
Ac-(PHGGGWGQ)$_4$-NH_2	Cu	120	n.r.	XO/NBT	6.6	[11]
Ac-HHGH-OH	Cu	130	n.r.	XO/NBT	6.8	[12]
H-HGDHMHNHDTK-NH_2	Cu	190	n.r.	XO/NBT	7	[13]
Ac-HVH-NH_2	Cu	200	n.r.	XO/NBT	7.4	[14]
(HPO_4)	Cu	1000	n.r.	XO/NBT	7.4	[14]

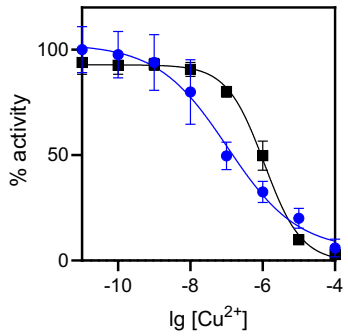

Fig. S16 | McCord-Fridovich assays showing the effect of ultracentrifugation on superoxide dismutase activity of Ac-HGIHIH-NH_2, with pre- (blue) and post- (black) centrifugation samples. Conditions: 200 µM peptide, 50 mM HEPES, pH 7.8

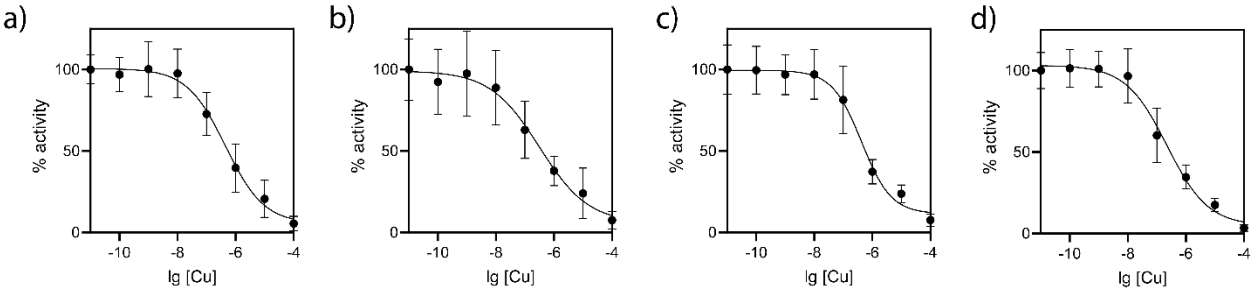

Fig. S17 | McCord-Fridovich assays a) Ac-HAAHVH b) Ac-HGFHVH-NH_2 c) L16 d) Ac-LHGIHIH-NH_2. Conditions: 200 µM peptide, 50 mM HEPES, pH 7.4

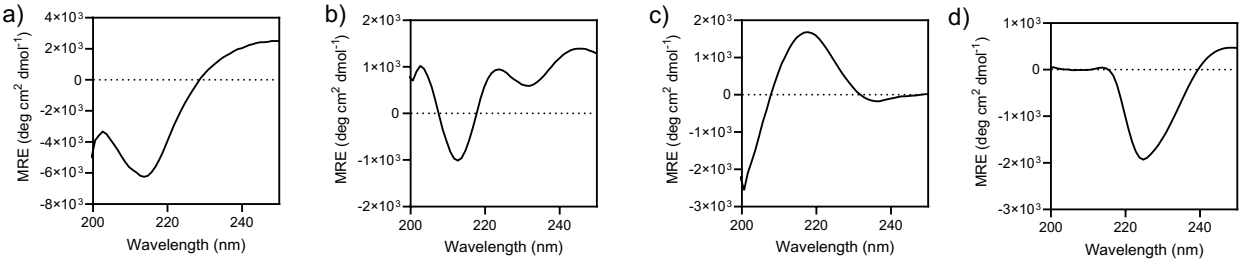

Fig. S18 | Circular dichroism spectra of peptide in the presence of Cu^{2+} ions. a) Ac-HAAHVH b) Ac-HGFHVH-NH_2 c) L16 d) Ac-LHGIHIH-NH_2. Conditions: 100 µM peptide, 100 µM Cu^{2+}, 5 mM HEPES, pH 7.4

References

1 Gleason, J. E. *et al.* Candida albicans SOD5 represents the prototype of an unprecedented class of Cu-only superoxide dismutases required for pathogen defense. *Proc. Natl. Acad. Sci. U. S. A.* **111**, 5866-5871 (2014).

2 Forman, H. J. & Fridovich, I. Superoxide dismutase: a comparison of rate constants. *Arch. Biochem. Biophys.* **158**, 396-400 (1973).

3 Shearer, J. Use of a metallopeptide-based mimic provides evidence for a proton-coupled electron-transfer mechanism for superoxide reduction by nickel-containing superoxide dismutase. *Angew Chem Int Ed Engl* **52**, 2569-2572 (2013).

4 Vincent, A. *et al.* An easy-to-implement combinatorial approach involving an activity-based assay for the discovery of a peptidyl copper complex mimicking superoxide dismutase. *Chem. Commun.* **56**, 399-402 (2020).

5 Kotynia, A. *et al.* The Analysis of Cu(II)/Zn(II) Cyclopeptide System as Potential Cu,ZnSOD Mimic Center. *Int. J. Pept. Res. Ther.* **23**, 431-439 (2017).

6 Csire, G. *et al.* Coordination, redox properties and SOD activity of Cu(II) complexes of multihistidine peptides. *J. Inorg. Biochem.* **177**, 198-210 (2017).

7 Dancs, Á., Selmeczi, K., Árus, D., Szunyogh, D. & Gajda, T. Catechol Oxidase and SOD Mimicking by Copper(II) Complexes of Multihistidine Peptides. *Int. J. Pept. Res. Ther.* **24**, 571-575 (2018).
8 Lihi, N., Kelemen, D., May, N. V. & Fábián, I. The Role of the Cysteine Fragments of the Nickel Binding Loop in the Activity of the Ni(II)-Containing SOD Enzyme. *Inorg. Chem.* **59**, 4772-4780 (2020).
9 Árus, D. *et al.* On the possible roles of N-terminal His-rich domains of Cu,Zn SODs of some Gram-negative bacteria. *J. Inorg. Biochem.* **106**, 10-18 (2012).
10 Mathieu, E. *et al.* Rational De Novo Design of a Cu Metalloenzyme for Superoxide Dismutation. *Chem. Eur. J.* **26**, 249-258 (2020).
11 Stańczak, P. & Kozowski, H. Can chicken and human PrPs possess SOD-like activity after β-cleavage? *Biochem. Biophys. Res. Commun.* **352**, 198-202 (2007).
12 Jancsó, A. *et al.* Solution chemical properties and catecholase-like activity of the copper(ii)–Ac-His-His-Gly-His-OH system, a relevant functional model for copper containing oxidases. *Dalton Trans.*, 3187-3194 (2005).
13 Paksi, Z. *et al.* Copper and zinc binding properties of the N-terminal histidine-rich sequence of Haemophilus ducreyi Cu,Zn superoxide dismutase. *J. Inorg. Biochem.* **102**, 1700-1710 (2008).
14 Bóka, B., Myari, A., Sóvágó, I. & Hadjiliadis, N. Copper(II) and zinc(II) complexes of the peptides Ac-HisValHis-NH2 and Ac-HisValGlyAsp-NH2 related to the active site of the enzyme CuZnSOD. *J. Inorg. Biochem.* **98**, 113-122 (2004).